The structure of a working catalyst ; from flat surfaces to nanoparticles
Roobol, S.B.

Cover Page

The handle http://hdl.handle.net/1887/29891 holds various files of this Leiden University dissertation

Author: Roobol, Sander Bas
Title: The structure of a working catalyst : from flat surfaces to nanoparticles
Issue Date: 2014-12-02

Chapter 6

NO reduction by H$_2$ over Pt nanoparticles studied by TEM

Where the previous chapter described an experiment in which we overcame the pressure gap for a simple catalytic reaction, the current chapter goes one step further and simultaneously overcomes the materials gap. The exposure of platinum nanoparticles to mixtures of nitric oxide (NO) and hydrogen (H$_2$) has been studied by *in-situ* Transmission Electron Microscopy (TEM). Similar to the faceting observed on the flat surface, we observe how material is transported and the particles change their morphology, depending on the gas composition. The particles have a faceted shape in hydrogen-rich environments, but lose their sharp corners in NO-rich environments and become more spherical.

6.1 Introduction

In the chemical industry a catalyst is never a flat surface, but rather a complex material that needs to be described at several different length scales, ranging from nanometres to at least millimetres[3]. In this chapter the smaller length scale is considered, namely that of the individual metal nanoparticles. Catalysis on small particles can be different from that on flat surfaces due to a variety of effects[6]. For example, on a small particle, there is a larger variety of adsorption sites and there are more undercoordinated metal atoms. Furthermore, spill-over effects can occur, both between the nanofacets on the particle and between the particle and support[8]. In addition, the electronic structure of the small particle can differ from that of the extended surfaces of the same material. Similarly, the interaction between the particle and the support can lead to further electronic effects[113].

The equilibrium shape of a crystalline particle is determined by the relative free energies of the terminating surfaces[114]. When the particle is in a gas environment, these are, in fact, the interfacial free energies between the metal surface and the gas phase and these depend heavily on the gas species present, on their partial pressures, and on temperature. The faceting of a platinum (110) surface into (320) and similar orientations, as described in the previous chapter, can be seen as a flat-surface analogue of this effect.

We have not found any publications describing *in-situ* studies on the interaction of platinum nanoparticles with NO. The closest are measurements on palladium particles during CO and NO cycling, where EXAFS, infrared spectroscopy, and mass spectrometry have been used to acquire indirect information on the particle shape, based on the observation that the palladium coordination is lowered during CO exposure and recovers in NO[115]. However, a later X-ray diffraction study proved this change in coordination to be caused by carbon dissolution from dissociated CO[116]. Similarly close is an environmental TEM (ETEM) study on CeO_2-supported platinum particles exposed to 1 mbar of CO, air, N_2 or O_2[117]. Whereas the platinum particles have a strongly faceted shape in vacuum and in N_2, the particles become somewhat rounded in O_2, and even more spherical in CO. A recent *in-situ* TEM study on the oscillatory behaviour of CO oxidation on platinum particles shows similar refaceting depending on the CO partial pressure[118].

6.2 Methods

Our TEM experiments have been performed with a micromachined nanoreactor[23, 119]. We have employed the latest generation of these devices, integrated on a single die[13]. It consists of a 0.5 μm deep gas channel etched in a silicon die, with electron-transparent windows that allow for in-situ TEM measurements of metal particles in
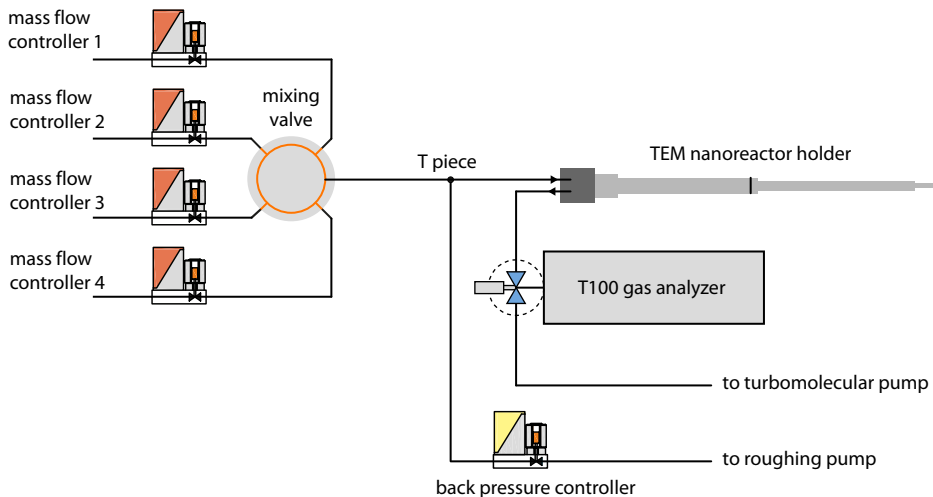
Figure 6.1. Schematic of the gas system to operate the nanoreactor in a flow configuration. The main flow path leads from the mixing valve via the T-piece and the back pressure controller to the rouging pump. Only a small fraction flows from the T-piece through the small nanoreactor channel and into the T100 analyzer[120]. When working at pressures beyond 1 bar (as set by the back pressure controller), the flow through the nanoreactor exceeds the maximum flow into the mass spectrometer of the T100 analyzer, and a turbomolecular pump is used to pump away the excess gas. This does not affect the time-resolution for gas detection thanks to the small volume of the inlet of the T100 analyzer. Note that the mixing system shown here is simplified and does not include the carrier gas.

a gas environment up to 14 bar and up to 800°C. The electron-transparent windows consist of a 15 nm amorphous silicon nitride film, and this film also coats the interior of the other parts of the channel, to ensure chemical inertness. Two viton O-rings connect the gas channel to a pair of capillaries in a dedicated TEM sample holder. A platinum heater is embedded in the nanoreactor directly above the gas channel and heats a small region around the electron-transparent windows, while simultaneously allowing temperature sensing by use of a calibrated resistance measurement.

The nanoreactor is operated in a flow configuration as shown in figure 6.1. Since the channel through the nanoreactor is extremely small (the reactor volume is 0.4 nl), the flow cannot be controlled by commercially available flow controllers. Instead, a certain gas pressure is set at the inlet, and the outlet is fed directly into a turbomolecular pump. To get a reasonable response time when changing the composition of the gas mixture, a gas flow is set up through a T-piece that is connected as close as possible to the inlet of the reactor and to a pressure regulator, backed by a vacuum pump. Most of the gas only flows through the T-piece and the pressure regulator, and only a small fraction flows through the reactor. The volume of the
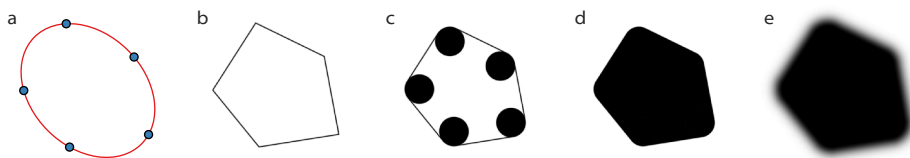
Figure 6.2. Construction of a polygon on a discrete grid, having rounded corners and a fuzzy boundary. (a, b) The corner points are defined by polar coordinates w.r.t. the center of the ellipse. (c) The inscribed circle is drawn at every corner. (d) The interior is filled using a hole-filling algorithm. (e) The edges are drawn with a gaussian intensity profile.

capillary between T-piece and reactor is large compared to the flow in this region, resulting in refresh times in the order of minutes. The gas stream is supplied by a gas mixing system[11, 56] that allows composing arbitrary mixtures of up to four gases plus a carrier gas at pressures up to 6 bar with a typical flow of 10 ml_n/min.

The outlet of the reactor is connected directly to a differentially pumped mass spectrometer (T100 gas analyzer[56]). The pressure drops entirely over the length of the nanoreactor since the gas channel in the nanoreactor is small compared to the diameter of capillaries leading to and from the reactor. The geometry of the nanoreactor is fully symmetric so it is assumed that the pressure in the central region of the nanoreactor (with the windows and heater) is half the pressure at the inlet. Since all gas from the reactor is pumped into the mass spectrometer (via the differential pumping stage), the sensitivity of the mass spectrometer is independent of the reactor pressure. The delay between an event in the reactor and detection by the mass spectrometer is approximately 30 s.

A platinum nanoparticle catalyst is loaded into the nanoreactor as a solution of tetraamine platinum nitrite in water or ethanol, which is left to dry in air, followed by calcination and reduction. In this process, the salt decomposes and the result is a dispersion of platinum nanoparticles with sizes ranging from 5 to 50 nm, inhomogeneously distributed in clusters along the entire nanoreactor gas channel.

The main conclusion reached in the present study is that Pt nanoparticles change their shape in response to the gas composition. As we will see, the most prominent feature is the sharpness of the edges and corners of the particles. Although it is relatively easy to recognise changes in the sharpness when visually inspecting sequences of TEM images, it takes effort to capture these variations in a robust, systematic, and quantitative way. We have developed a new method especially for this purpose, based on the least-squares fit of a 2D model, which is illustrated in figure 6.2 and described in detail in appendix 6.A in this chapter.

6.3   Results and discussion

Figures 6.3, 6.4 and 6.5 show an ensemble of Pt particles that we followed during its first exposure to NO after sample preparation. Starting from 1 bar pure H_2 at 150°C, the inlet gas composition was first changed to NO. As explained above, the low refresh rate of the gas in the capillary leading to the nanoreactor inlet translated to a gas composition change in the reactor starting after a delay of 2 minutes and with a transition time of another 2 minutes. Two dramatic effects are immediately visible in the TEM images. The number of nanoparticles has decreased and the remaining particles have become rounder in the NO atmosphere.

The number of Pt particles started decreasing as soon as the NO partial pressure in the reactor was increasing (figure 6.4) from t = 200 s. The TEM images obtained during the next two minutes show that small particles were shrinking. Although the bigger particles showed no clear change in size, they probably accommodated the Pt lost from the smaller particles. These observations indicate that individual atoms were diffusing over the support between the Pt nanoparticles, resulting in a net flux from the smaller to the larger particles. This mechanism is known as Ostwald ripening[121]. The alternative mechanism of Smoluchowski ripening in which entire nanoparticles diffuse and merge[122], can be ruled out. Since the process is not reversible, a systematic study of the effects of gas composition on the ripening rate and mechanism was not performed in the context of this first in-situ experiment on the effect of high-pressure H_2 and NO atmospheres on Pt nanoparticles. The dramatic increase of the ripening rate of Pt particles induced by NO has been reported by Lööf and co-workers[123]. They found that the effect of NO is stronger than that observed for O_2, which already enhanced the ripening compared to H_2 and Ar. They suggest that an NO-containing Pt complex is the mobile species responsible for the fast ripening.

The second effect observed in the experiment is the reversible change in the particle shape depending on the gas composition. This effect could be reproduced repeatedly in two different nanoreactors loaded with Pt particles. In order to substantiate our visual impression of systematic variations in particle shape with gas composition, we have quantitatively analyzed the shapes of some of the larger particles in the ensemble using the fitting procedure described in appendix 6.A of this chapter. Figure 6.5 shows the result. The lower panel displays the best-fit values of the corner rounding radius as function of time. Although the rounding radius is noisy, a correlation with the NO partial pressure is visible: higher NO pressures correspond to more rounded particles. There are two reasons for the noise on the radius. One is the low contrast between particle and background, resulting from the necessity to work with a low electron dose. The other is the spatial inhomogeneity of the amorphous SiN nanoreactor windows, which makes the background noisy. As a result, the fitting procedure did not always converge reliably. For some parameters,
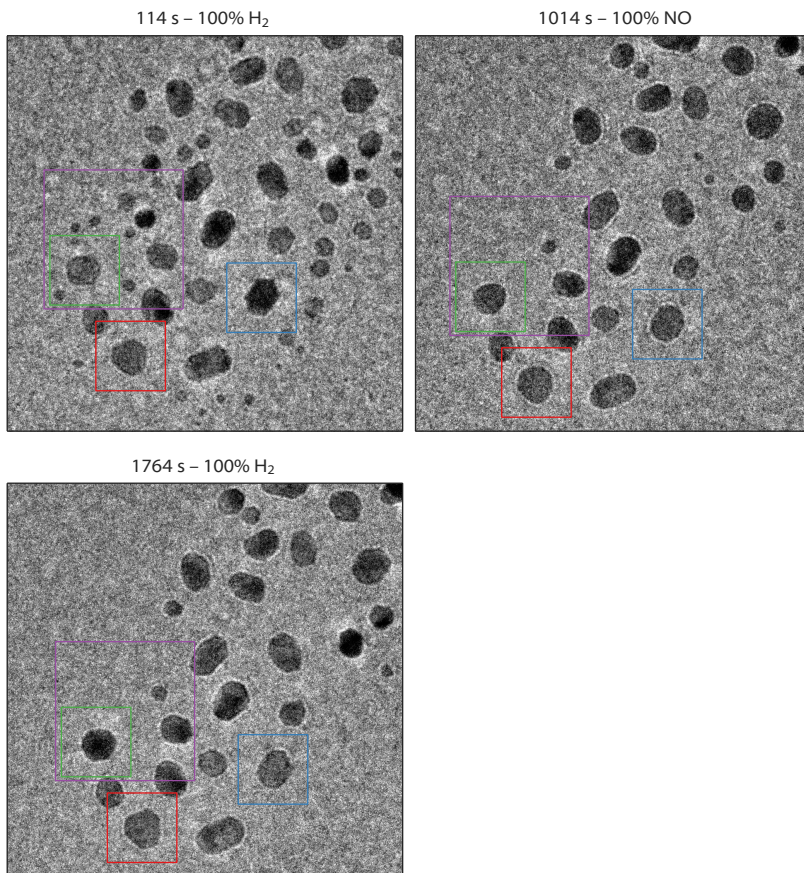
Figure 6.3. Shape variations of Pt particles while the gas composition was varied from pure H$_2$ (upper left panel) to pure NO (right panel) and back (lower panel), at 1 bar and 150°C. An ensemble of particles has been imaged every 3 seconds with an acquisition time of 1 second per frame. The imaging started at $t = 0$ in pure H$_2$, see the lower panel of figure 6.5 for more detail on the timing of the gas changes. The sample was continously exposed to an electron dose of 300 e/Å^{2}s at 300 keV. The size of the images is 92×92 nm^2. Three particles, indicated with red, blue and green rectangles, are analyzed in more detail in figure 6.5. Note the sintering taking place between the left and middle panels (purple rectangle), which is shown in more detail in figure 6.4.
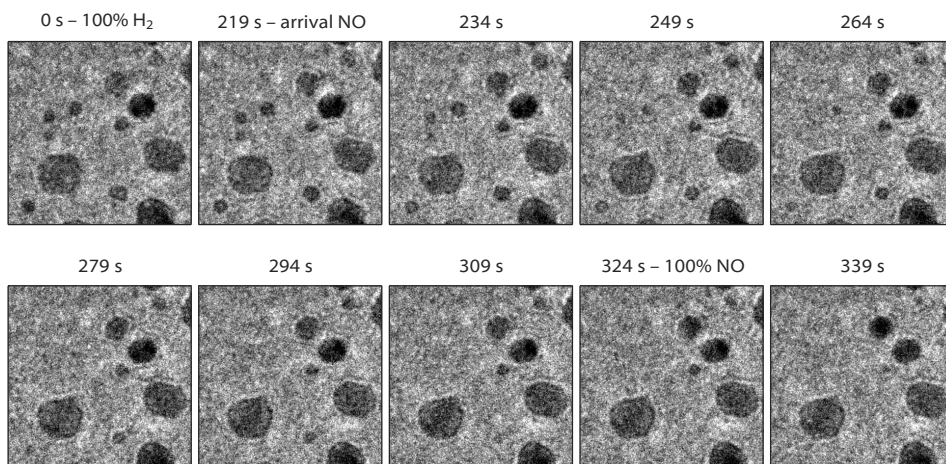
Figure 6.4. Rapid ripening took place at 150°C when NO was flowed through the reactor. The initial hydrogen atmosphere did not result in any noticable evolution, but once the NO partial pressure started increasing (from t = 219 s), the particles changed in size. Small particles shrank and disappeared on a time scale of tens of seconds, larger particles seemed unaffected, within the resolution of the images. This indicates that the mechanism of the process is Ostwald ripening. The images correspond to $32 \times 32 \text{ nm}^2$ cutouts of the larger images, such as those in figure 6.3.
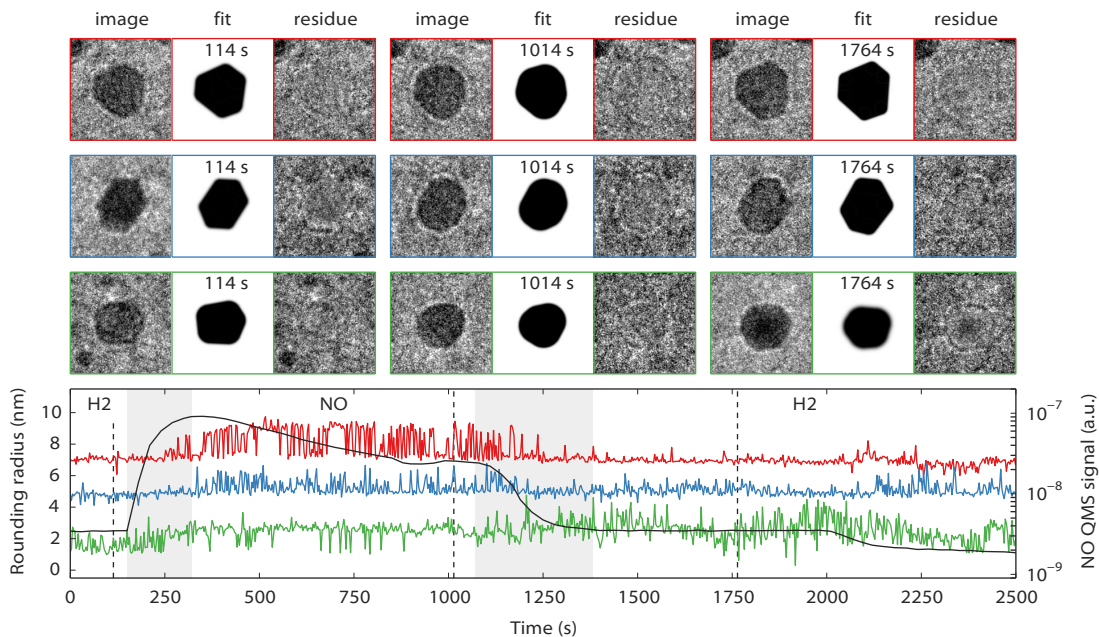
Figure 6.5. Three particles from the ensemble of figure 6.3 that have been analysed with the fitting procedure (upper panel / red, middle panel / blue, and lower panel / green), each image corresponds to $16 \times 16\ \text{nm}^2$. The graph in the lower panel shows the rounding radius of the corners, as determined by the fit (offset from zero by 6 and 4 nm for red and blue respectively). The gas composition is indicated by the labels and the black curve in the lower panel, the two grey sections correspond to transitions from one gas to another. Note that the sensitivity of the quadrupole mass spectrometer (QMS) to NO reduced in time, due to the gain of the electron multiplier being affected by the gas in the QMS chamber. For each particle, the raw data, the fit as determined by the least-squares optimization, and the residue (raw image minus fit) are shown at three different points in time, corresponding to the vertical dashed lines in the graph. The model does not incorporate the Fresnel scattering on the edges of the particles, and this causes the boundaries of the particles to remain visible in the residue. Note the correlation between the presence of NO and the rounding radius, both in value and noise level.

especially the rounding radius, the final value strongly depends on the initial values. The two-level character of the rounding radius is caused by the upper limit of the rounding radius (approximately the particle radius) that was enforced by the fitting procedure.

6.4 Conclusion

In our high-pressure TEM observations we have witnessed two effects of the presence of NO in the gas mixture on ensembles of Pt nanoparticles. NO leads to a rapid ripening of the ensemble, with smaller particles shrinking and disappearing, i.e. Ostwald ripening. Furthermore, the particles become more rounded in the presence of NO. The latter effect can be viewed as the particle analogue of the break-up of the Pt(110) surface into vicinal orientations, that was discussed in the previous chapter. The explanation hypothesized there, namely that the adsorption-induced surface stress on the low-index terraces is reduced by the introduction of a high density of steps, could also be at play at the (111) and (100) surfaces, thus reducing the size of all facets and introducing larger vicinal regions, the rounded corners, on the nanoparticles. Since the steps that are introduced via the adsorption-induced stress scenario provide strongly coordinating adsorption sites with potential catalytic benefits, this mechanism may be of direct practical relevance for the performance of catalytic nanoparticles under high-pressure conditions.

6.5 Outlook

It would be interesting to determine the dependence of the rounding on the NO pressure, or rather on the chemical potential. In the previous chapter discussing the Pt(110) surface we reported that different NO partial pressures seem to induce different vicinal surfaces, e.g. (320) or (540). This suggests that the precise roundness of the nanoparticle will depend sensitively on the NO pressure. Assuming that only the chemical potential of the adsorbate species plays a role and not kinetics, this could be similar to what Yoshida and coworkers reported for CO on Pt particles[117]. They found that when exposing initially faceted Pt particles to 1 mbar CO at room temperature, the particles become round, and when increasing the temperature to 200°C this effect weakens.

Thus, repeating the experiment at lower NO pressures would be a logical next step. With the nanoreactors it is difficult to probe the mbar regime and below, but this is the regime where the use of ETEM is well established, so it is possible to cover several orders of magnitude in pressure. A higher signal-to-noise ratio of the TEM images than shown in this chapter is needed to capture the fine details in the shape of the particles. Since there are no dynamic processes that need to be followed, this

is feasible without increasing the electron beam intensity to avoid beam effects, by using longer exposures, or preferably averaging series of short-exposure images to avoid resolution loss due to drift.

Appendix 6.A   Particle shape analysis

When exposing the platinum particles to varying ratios of NO and H_2 mixtures it became clear that it was desirable to quantify changes in particle shape. We have developed a new fitting method that quantifies the degree to which the corners of a faceted nanoparticles are rounded. This method does not rely on edge detection, contrary to other methods for analysing TEM images of particles described in literature[117, 118]. In those methods, the precise location of the contour of a particle is established, and a curve fitting procedure is used to obtain the optimal fit of a 1D curve in a 2D space. The weak element in these methods is the edge detection, which is a non-trivial operation, contrary to what is implied in these publications. In addition, the edge detection fails if the signal-to-noise ratio is low, as is the case in the dataset at hand in the present chapter. In this case the low signal-to-noise ratio is caused by the electron-transparent nanoreactor windows that give a speckled background pattern, and the low electron dose required to minimise beam effects. We use a least-squares optimization to fit a 2D simulated particle silhouette to a TEM image, or equivalently, fit a 2D surface in a 3D space, thus avoiding edge detection completely.

We first describe the geometrical construction of the rounded polygon and then show how this is translated into a matrix of greyscale values on a discrete grid, matching the pixels of a TEM image.

The number of corners of the polygon N is assumed to be fixed and not a fit parameter. The degrees of freedom for the corner positions should be limited, e.g. to avoid concave polygons. Therefore it is assumed that all corners of the polygon are located on an ellipse, as is shown in figure 6.2a. The ellipse is described by two radii (a, b), the center coordinates (x_0, y_0), and an orientation angle ϕ of the major axis. The position of the corners can then be specified as a list of angles $(0 \leq \alpha_1 < ... < \alpha_N < 2\pi)$.

In the absence of rounding, the polygon is simply formed by the N straight lines connecting neighboring corner points (figure 6.2b). Rounding is introduced via a single corner radius r for all N corners of the particle, as illustrated in figure 6.2c. The straight line segments then terminate at the tangent points to the inscribed circles at each corner. Next, the interior of the rounded polygon is filled (figure 6.2d). At this stage, the silhouette has sharp edges whereas the TEM images show edges that are somewhat blurred. This aspect needs to be taken into account. There is a second reason for blurring the sharp edge, namely to translate the mathematical shape of

figure 6.2d in to a non-jagged grid representation that evolves continuously under variations in the corner position and corner rounding radius (even for variations smaller than the size of a pixel). For this purpose, we make the pixel greyscale values for pixels outside the silhouette drop off with the distance to the nearest point on the contour of the rounded polygon according to a Gaussian with a width σ (figure 6.2e). This approach ensures continuity of the least-squares error χ in all parameters when σ is not much smaller than the pixel size.

The result of figure 6.2e is scaled and an offset is added to match the background and foreground intensities of the TEM image. The entire procedure has $9 + N$ parameters and results in a least-squares error χ that is not only continuous but also differentiable with respect to these parameters, with the exception of the rounding radius parameter r, which clips at an upper limit depending on the particle size. This upper limit is given by the radius of the largest inscribed circle (at every corner) that fits within the enclosing polygon and this approximately matches the particle radius.

We use a least-squares optimization procedure based on a steepest-descent algorithm from Scipy[52]. Due to the low signal-to-noise ratio in the dataset in this chapter, the procedure did not always converge to a shape that properly describes the particle, and manual tuning of the starting values was required. This can likely be improved by tailoring the optimization algorithm to this particle model and its choice of the parameters, but this has not been attempted. The fit procedure typically takes up to one minute on a 2.8 GHz Intel Core i7 CPU to converge for a 80×80 pixel image.